IOP Publishing Journal of Geophysics and Engineering
J. Geophys. Eng. **14** (2017) 698–712 (15pp) https://doi.org/10.1088/1742-2140/aa63bf

The magnetotelluric response over a 3D polarizable structure

R Esposito[1], A Troiano[2], M G Di Giuseppe[2], D Patella[2,3] and R M Castelo Branco[1]

[1] Federal University of Ceará, Fortaleza, Brazil
[2] Osservatorio Vesuviano, Istituto Nazionale di Geofisica e Vulcanologia, Naples, Italy
[3] Department of Physics, University Federico II of Naples, Italy

E-mail: roberta.esposito@ov.ingv.it

Received 29 June 2016, revised 23 February 2017
Accepted for publication 1 March 2017
Published 27 April 2017

Abstract

This paper analyses the 3D magnetotelluric (MT) response in the presence of resistivity frequency dispersion. The aim is to give further insight into this topic, already approached in previous papers dedicated to 1D and 2D cases. We show the MT diagrams along three parallel profiles, normal to the longitudinal axis of a dispersive conductive prism of finite horizontal and vertical extent, buried in a non-dispersive resistive half-space. The Cole–Cole dispersion law has been assumed to represent the dispersion features of the prism. The MT responses along the same profiles in the complete absence of dispersion effects are also provided for reference. The results confirm that the TE mode, as in the 2D case, is mostly affected by dispersion. Compared with the non-dispersive responses, a notable increase in the amplitude of the anomaly is observed along the profile passing through the center of the prism, while an increase in its width is the effect along the profile above the edge of the prism. As a field example, the MT profile in the eastern Snake River Plain geothermal area is considered. The profile was already dealt with in a previous paper by a 2D dispersive MT modeling approach, by which a dispersive slab of infinite length in the direction normal to the MT profile, immersed in a 1D layered host, was modeled. A finite length of the dispersive conductive slab is now derived, validated by the increased goodness of fit between the field TM and TE pseudosections and the synthetic ones from the 3D model compared with the misfit previously obtained by the 2D approach. Finally, an explanation of the chargeability and main values of the time constant assumed to fit the field data is attempted in terms of the abundance of hydrothermal alteration products and temperature, respectively, inside the dispersive slab.

Keywords: resistivity frequency dispersion, magnetotelluric response, 3D structures

(Some figures may appear in colour only in the online journal)

Introduction

Resistivity dispersion constitutes the basis of the prospecting method of induced polarization (IP) and is a widely known phenomenon in geophysics (Seigel 1959, Wait 1959, Bertin and Loeb 1976, Sumner 1976, Fink *et al* 1990). In the frequency domain (FD), electrical resistivity changes with the variation of the frequency of the exciting current. The dispersive resistivity, called impedivity (Patella 1993) is a complex function of frequency. When frequency tends to zero or to infinity, however, the impedivity is real and corresponds to the classical resistivity parameter of DC geoelectrical methods.

The IP FD spectrum in rocks is mostly modeled using the Cole–Cole type of impedivity function $\rho^{CC}(\omega)$ (Cole and Cole 1941), given as

$$\rho^{CC}(\omega) = \rho_0\{1 - m[i\omega\tau^c/(1 + i\omega\tau^c)]\}. \quad (1)$$

In equation (1), $i = \sqrt{-1}$, ω is the angular frequency, ρ_0 is the DC resistivity and $m \in [0, 1]$, which is known in mining geophysics as chargeability (Seigel 1959), is the IP amplitude, defined as $m = (\rho_0 - \rho_\infty)/\rho_0$, where $\rho_\infty \in [0, \rho_0]$ is the resistivity at infinite frequency. Furthermore, $c \in [0, 1]$ is the flattening factor of the decay spectrum and $\tau \geqslant 0$ is the main time constant.

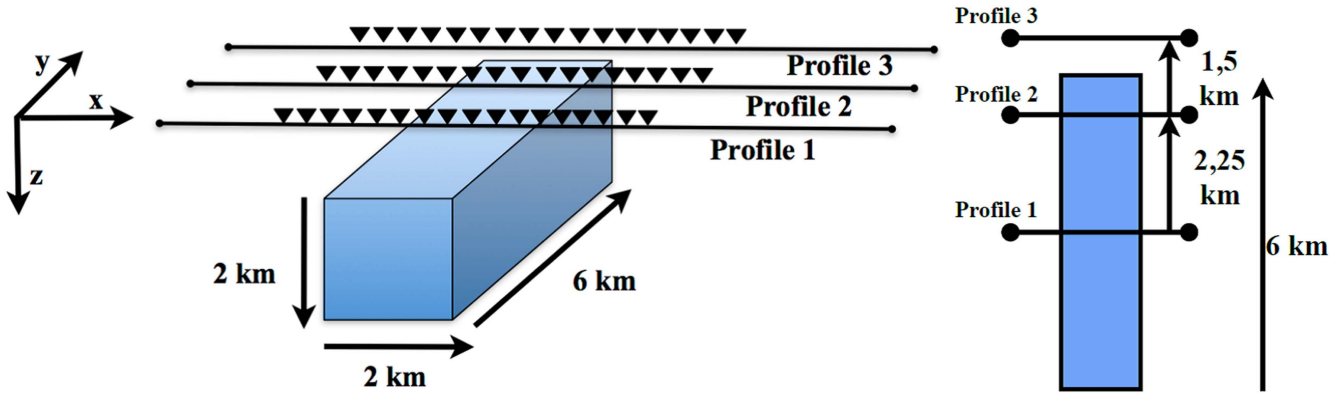

Figure 1. Left: the 3D model and the selected profiles with corresponding station sites. Right: the model seen from above.

Stoyer (1976) and Patella (1987) have shown that the dispersion of the resistivity can affect the magnetotelluric (MT) response. The detection and the spatial definition of impedivity effects can significantly improve the understanding of the physical properties of rocks, enabling exploration to depths well beyond the extent of standard IP equipment, typically a few tens of metres.

Magnetotellurics is an ideal technique to detect high-dispersion zones in applied fields such as hydrocarbon and geothermal exploration. These zones are typically highly fractured and pervasively altered, owing to the chemical interactions of the rocks with the uprising light hydrocarbons and hot fluids. Such zones are reliable indicators of the presence of exploitable reservoirs below.

Following the theory developed by Patella (1987, 1993), the Cole–Cole model was included in MT theory to study the distortions provoked by dispersion on 1D (Patella 1987, Esposito and Patella 2009) and 2D (Mauriello *et al* 1996) synthetic responses. Dispersion effects in MT theory were recognized experimentally and modeled by 1D and 2D tools in volcanic and geothermal areas (Patella *et al* 1991, Coppola *et al* 1993, Giammetti *et al* 1996, Di Maio *et al* 1997, 2000, Mauriello *et al* 2000, 2004) and in hydrocarbon exploration (e.g., He *et al* 2010).

The purpose of this paper is to further study the influence of the resistivity dispersion in MT theory by analyzing the synthetic responses generated by a 3D body. We mention that 3D IP effects have gained widespread interest also in TDEM, FDEM and LOTEM prospecting, as documented in many recent papers (e.g., Chang-Chun and Bin 1994, Hoheisal *et al* 2004, Zaslavsky *et al* 2011, Marchant *et al* 2014). In the present MT simulation, the 3D body is a dispersive conductive prism immersed in a non-dispersive resistive half-space. This contrast in resistivity is motivated by previous simulations on 1D and 2D models. Dispersive conductive layers sandwiched between dispersion-free resistive layers (1D), and dispersive conductive, infinitely long prisms hosted in a dispersion-free resistive half-space (2D) have shown the most remarkable distortions (Mauriello *et al* 1996, Esposito and Patella 2009). Moreover, such a model, with a proper choice of the prism's size and depth, can be useful in interpreting MT data when prospecting for oil and geothermal reservoirs (Zhdanov and Keller 1994, Pellerin *et al* 1996).

An MT field dataset, related to a geothermal exploration program in the eastern Snake River Plain, Idaho (Stanley 1982), is reanalyzed within a 3D framework, in order to highlight the greater interpretative potential that rises from the inclusion of 3D dispersion effects in MT data analysis.

For brevity of the text, we omit the recall of known basic MT formulas. The reader is referred to Mauriello *et al* (1996) for the inclusion of the dispersion phenomenology in MT theory.

3D simulation of dispersive effects in MT theory

Figure 1 shows the 3D model assumed for studying the IP effects in MT. A horizontal dispersive prism with resistivity $\rho_0 = 10\,\Omega$ m is buried in a non-dispersive half-space with resistivity 200 Ω m. The 3D body has a horizontal length of 6 km along the *y*-axis and square edges of $2 \times 2\,\text{km}^2$. The top face is located at a depth of 2 km.

The simulations have been done along three 8 km long profiles parallel to the *x*-axis. Profile 1 crosses the prism's mid-length, profile 2 is 2250 m apart from profile 1, and profile 3 is 1500 m apart from profile 2 (figure 1). Seventeen MT station points, spaced 500 m apart, have been assumed along the profiles. The frequencies 10, 1, 0.1, 0.01 and 0.001 Hz have been taken to plot the modulus and phase of the MT apparent impedivity functions of the TE and TM modes, in order to show how IP alters the MT profiles with decreasing frequency, i.e. with increasing penetration depth.

For the sake of conciseness, only one example of a simulation is presented, and it refers to the following Cole–Cole parameter set for the dispersive prism: $m = 0.9$, $\tau = 10$ s and $c = 0.75$ (figures 2–4). In all figures, the blue lines refer to the reference non-dispersive case and the red lines to the dispersive assumption.

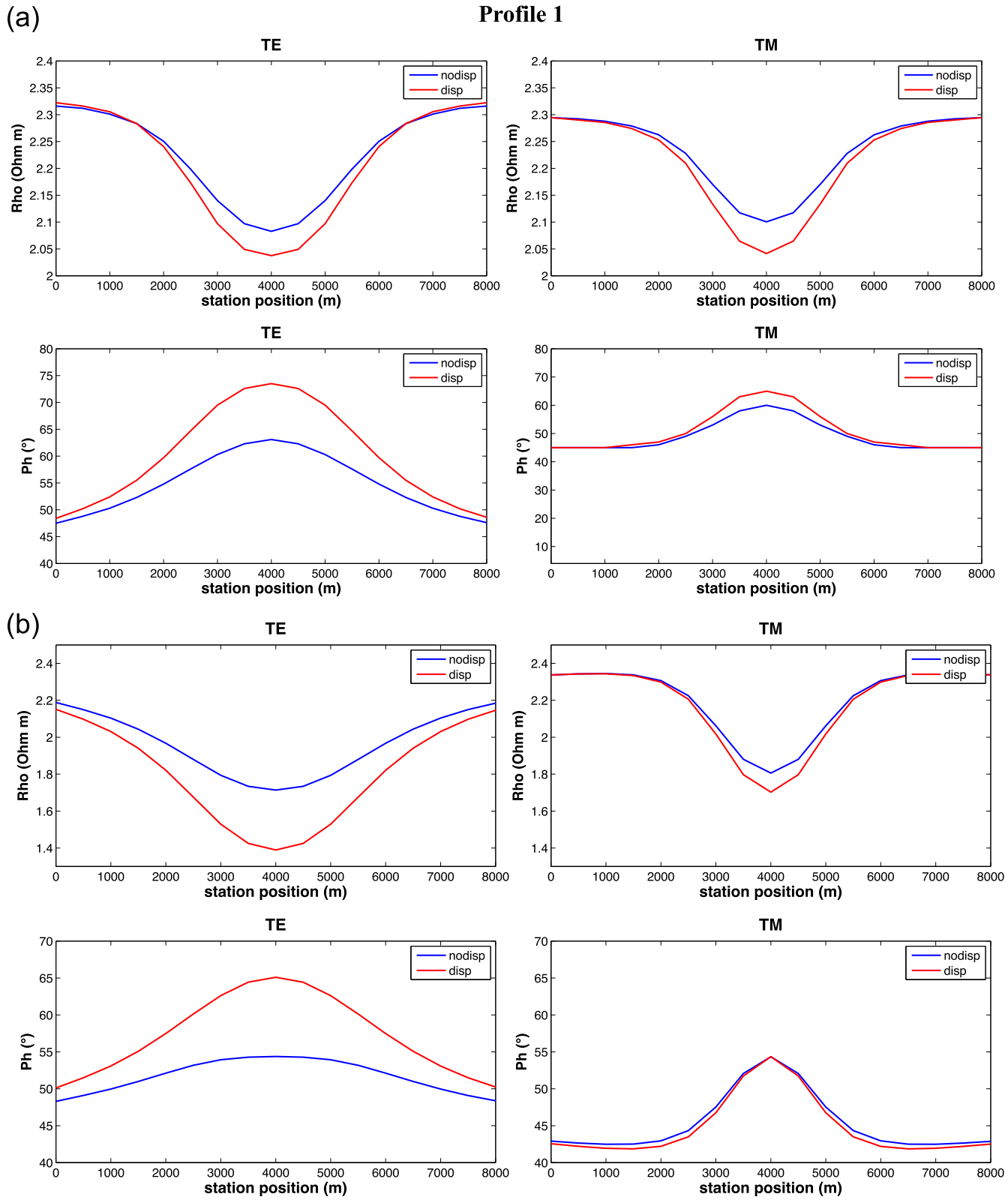

Figure 2. Modulus (top diagrams, in Ω m) and phase (bottom diagrams, in deg) of the two orthogonal TM and TE modes of the MT apparent impedivity response against distance (in m) along profile 1, calculated at various frequencies. The blue curves refer to the reference non-dispersive response, and the red curves to the dispersive case. Frequencies: (a) 10 Hz, (b) 1 Hz, (c) 0.1 Hz, (d) 0.01 Hz, (e) 0.001 Hz.

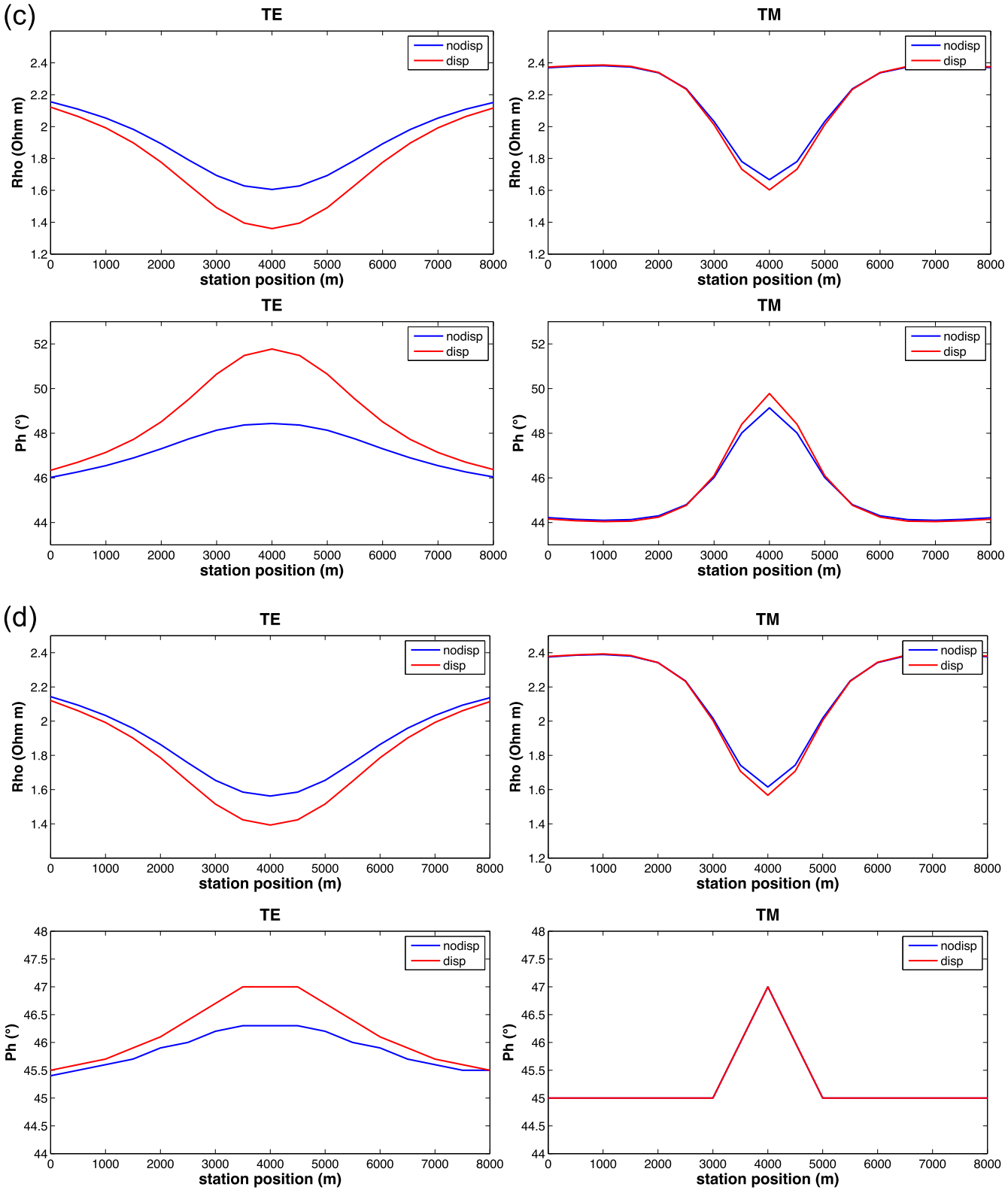

Figure 2. (Continued.)

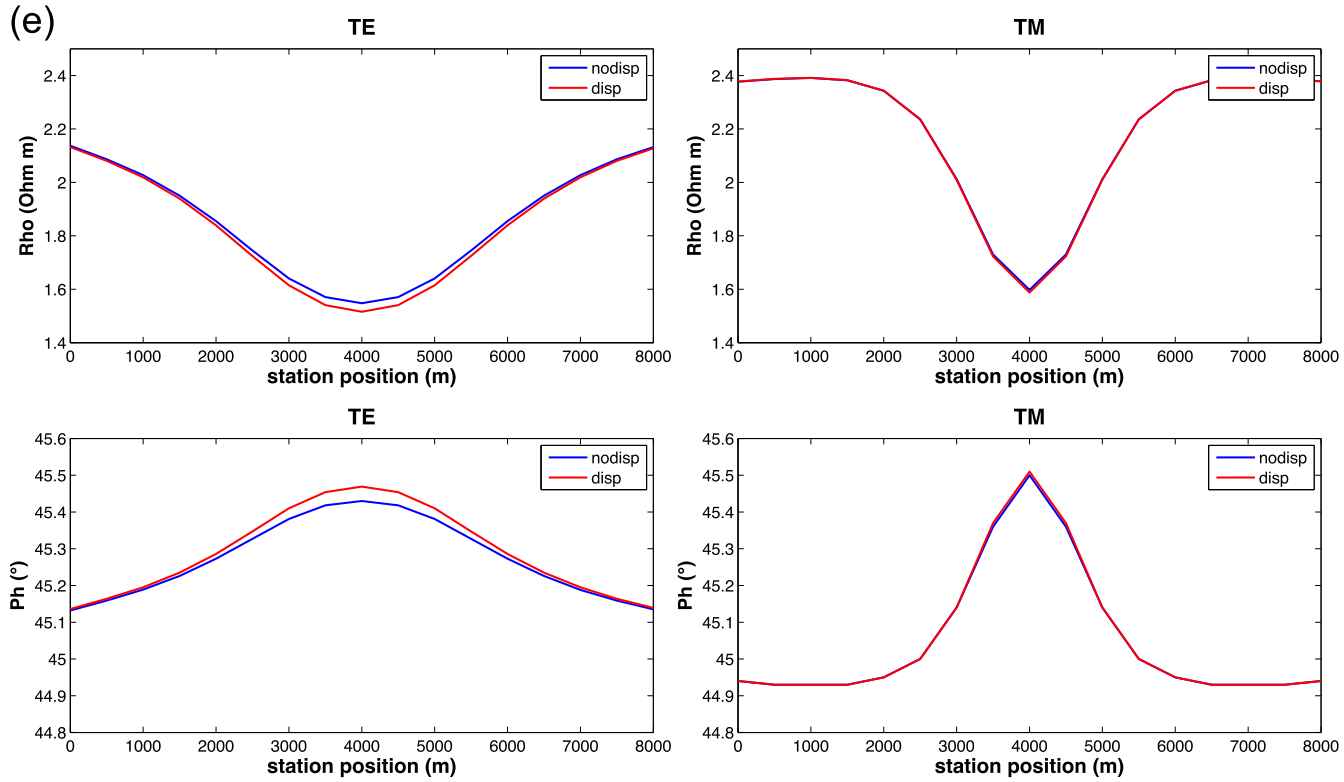

Figure 2. (Continued.)

The following features are detected. Along profile 1, centered over the prism (figure 1), the departure of the red lines from the reference blue lines, for both modulus and phase of the TE and TM modes, is very evident. The IP effect is manifested with a more pronounced minimum of both the TE and TM apparent impedivity modulus, centered above the median axis of the 3D dispersive body. The departure from the reference non-dispersive profiles starts to grow from 10 Hz, reaches its maximum at 1 Hz, then slowly decreases as frequency decreases, until it almost disappears at 0.001 Hz. A specular character is observed in the phase curves, where the dispersion-related red lines show a magnified maximum with respect to the non-dispersive reference blue lines. For all frequencies the more vigorous effect is observed in the TE mode.

Along profile 2, the behavior of the curves appears similar to that along profile 1. However, two differences can readily be discerned. The first is that the departure of the dispersive red curves from the non-dispersive blue curves is less pronounced than in the previous case. The second difference regards mainly the TE mode and does not depend on dispersion. It consists in a symmetrical slope reversal in the central portion of the anomaly, with the appearance of peaks corresponding to the median longitudinal axis of the prism. This effect is likely due to the influence of the nearer vertical square face of the prism.

Finally, along profile 3, the effect of dispersion as seen along profiles 1 and 2, i.e. the increasing amplitude of the minima and maxima along the dispersive red curves, almost completely disappears. The different width of the anomaly centered above the prism becomes the dominant character instead, especially for the curves of the modulus. The red central anomalies at 1 Hz are narrower than the corresponding blue anomalies; then, from 0.1 Hz down to 0.001 Hz, the red anomalies gradually become wider than the blue ones.

Of course, the amount of distortion of the MT response over a polarizable body depends on the values assigned to the Cole–Cole parameters, m, τ and c. Values of m in the range 0.4 to 0.9, of τ in the range 10^{-3} s to 10^{4} s, and of c in the range 0.1 to 0.8 are reported in the literature from laboratory and field experiments made with full spectral or multi-frequency IP methods (e.g., Keller and Frischknecht 1966, Sumner 1976, Pelton *et al* 1978). Mauriello *et al* (1996) gave a detailed overview on this topic, and inferred from 2D simulations that high values of m (not less than 0.75) and τ (not less than 100 s) are ideal for dispersion effects to be recognizable in MT measurements. They also showed that the TE is always the most distorted MT mode. Esposito and Patella (2009) showed that c has practically no remarkable distortion effect in the MT effect on 1D structures. The small influence of c was also inferred by Mauriello *et al* (1996) in 2D cases. The above effects have also been tested within the present study devoted to 3D structures. The results from a great number of simulations on the model in figure 1, carried out following the same approach as in Mauriello *et al* (1996)

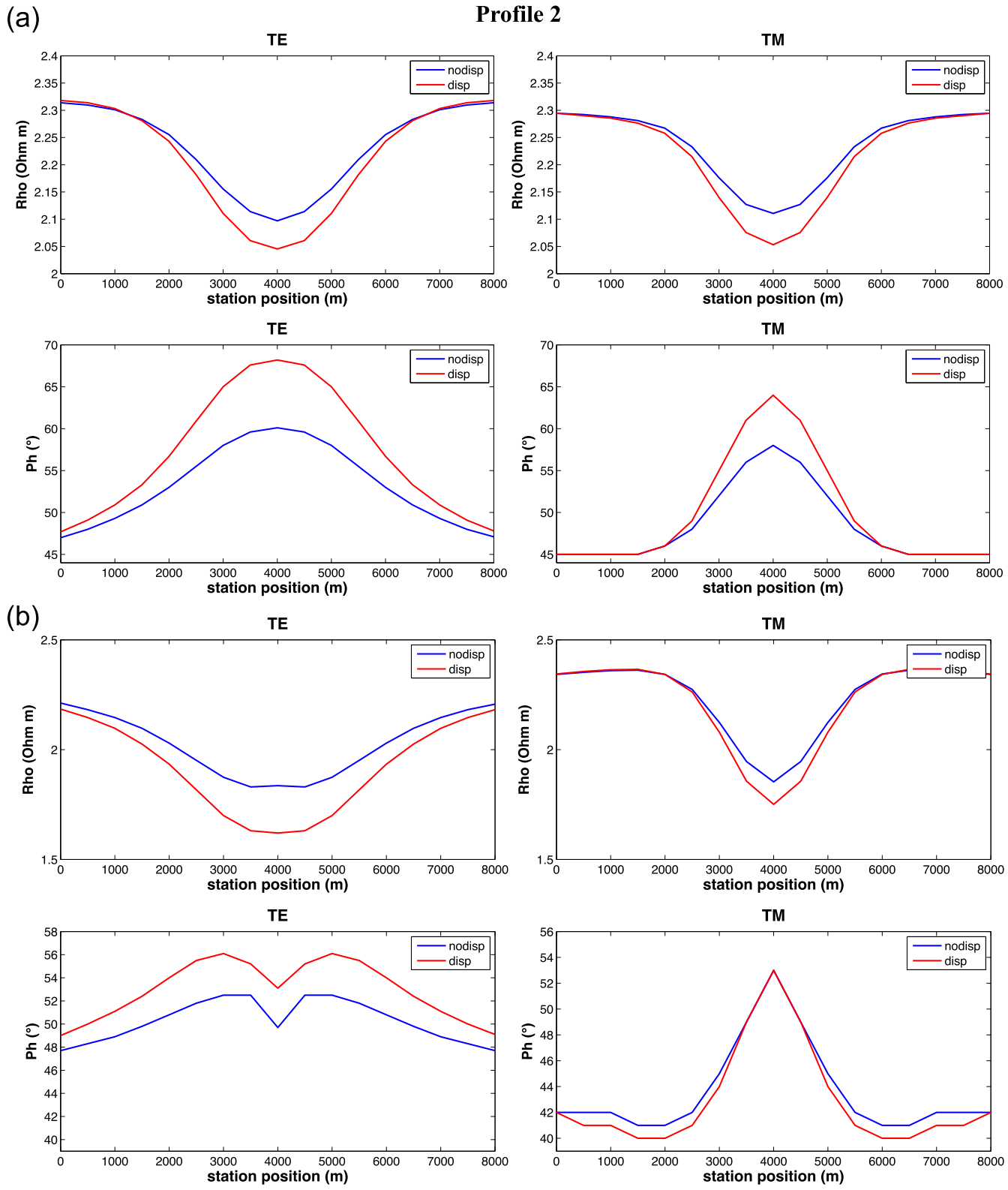

Figure 3. Modulus (top diagrams, in Ω m) and phase (bottom diagrams, in deg) of the two orthogonal TM and TE modes of the MT apparent impedivity response against distance (in m) along profile 2, calculated at various frequencies. The blue curves refer to the reference non-dispersive response, and the red curves to the dispersive case. Frequencies: (a) 10 Hz, (b) 1 Hz, (c) 0.1 Hz, (d) 0.01 Hz, (e) 0.001 Hz.

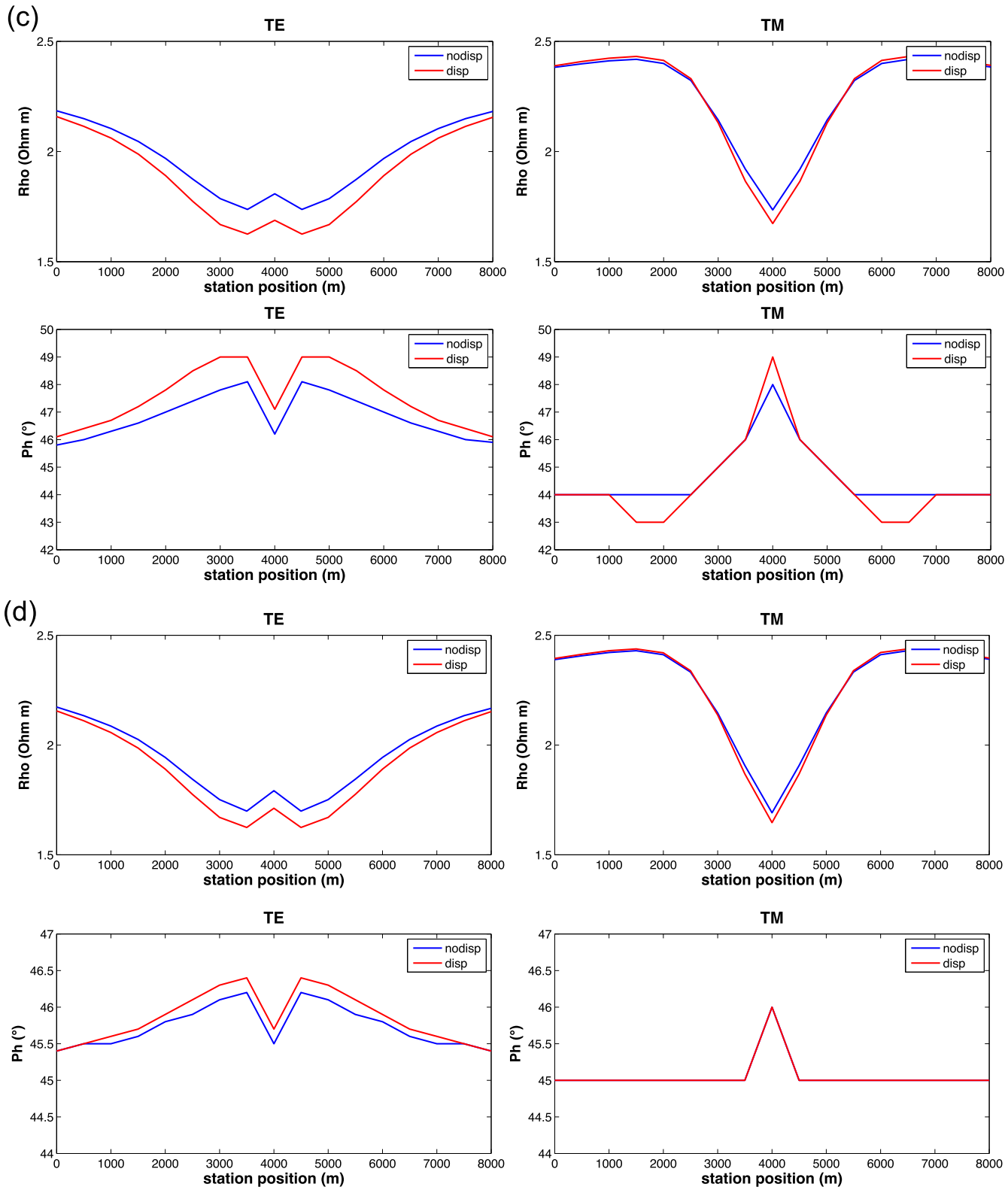

Figure 3. (Continued.)

by changing m and τ with fixed c, fully confirm all of the above conclusions. A further consideration is that visible distortion effects can be obtained even when m and τ vary in opposite directions. The sense is that the choice of an exceedingly low value of one of them must be compensated by a quite high value of the other. This is just the case we have discussed a few lines above, where the value $\tau = 10$ s—well below the lower limit of the range of τ previously

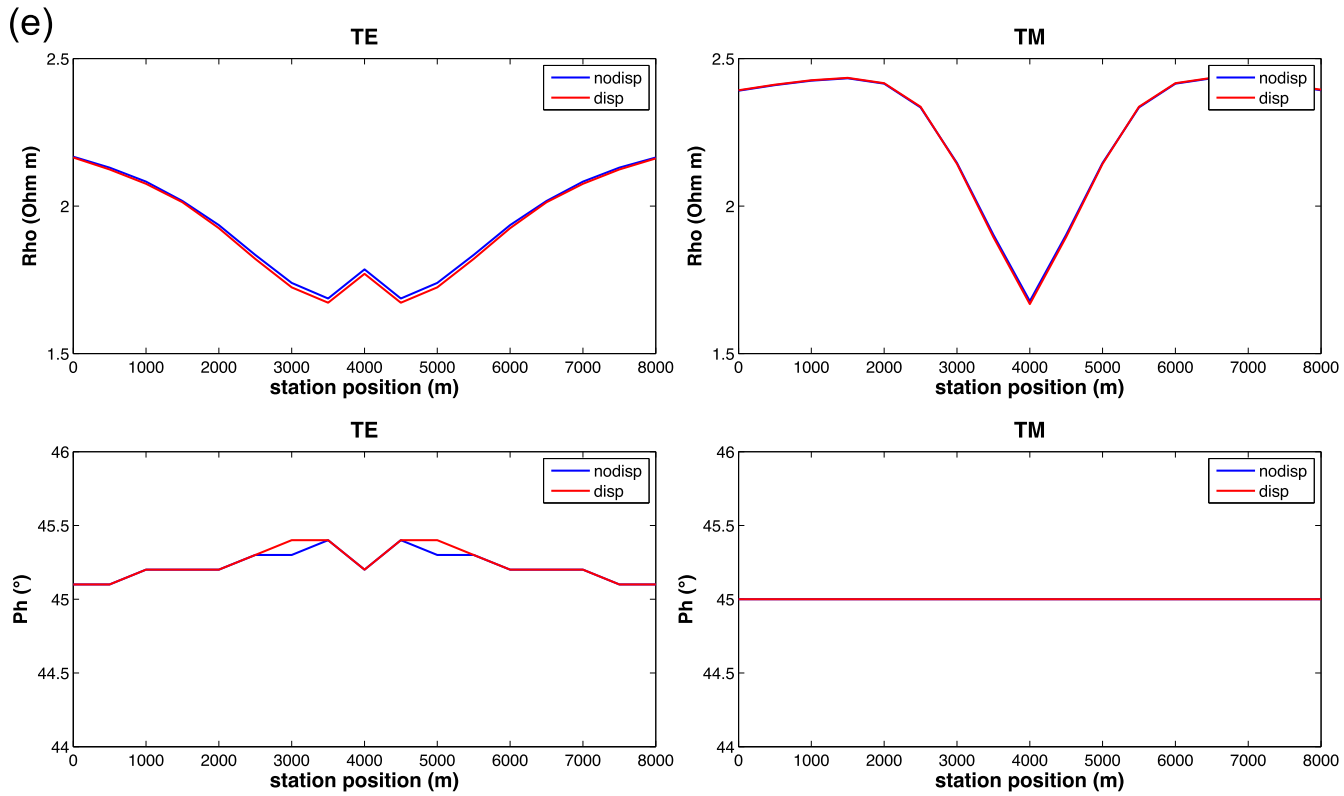

Figure 3. (Continued.)

recalled—is compensated by the value $m = 0.9$, at the top limit of the range of m.

Field example

We now show a field example already studied by Mauriello and Patella (1999) in the framework of imaging using probability tomography. The area is the eastern Snake River Plain (SRP), Idaho, where an MT profile was performed by Stanley (1982) near the Idaho National Engineering and Environmental Laboratory (figure 5). Figure 6 shows the TM and TE apparent resistivity pseudosections across the MT profile of the SRP.

The SRP is an arcuate depression bounded on both sides by the Basin and Range structures, and for much of its extent it is underlain by basalt and interbedded continental Quaternary and Tertiary sediments (Mabey 1982). Mauriello and Patella (1999) applied 2D probability tomography imaging to the TM and TE pseudosections of the SRP shown in figure 6 and evinced within the SRP depression a laterally bounded conductive slab with a lateral extent of about 17 km and a mean depth to its top of about 2 km.

Dispersion effects were also admitted, in order to explain the occurrence of a charge polarity inversion at the top edges of the slab and a tightening of the same edges as frequency decreases. Using the 2D dispersive MT forward modeling by Mauriello *et al* (1996), the 2D structure depicted in figure 7 was then proposed, as best conforming to the large-scale geometry and dispersion inferences from the probability tomography sections. Finally, by comparing the synthetic TM and TE pseudosections from the 2D model in figure 7 with the original ones in figure 6, Mauriello and Patella (1999) found a good matching of the two TM pseudosections, while the TE ones were judged not to properly conform to each other. They attributed this discrepancy to the circumstance that the TE mode is much more affected than the TM mode whenever a 2D geometry is assumed to approximate a slab of limited strike length (Wannamaker *et al* 1984, 1997, Livelybrooks *et al* 1996).

We now propose a 3D refinement of the 2D section in figure 7, using the same resistivity sequence and Cole–Cole parameters as in the 2D model and assigning after trial-and-error a final strike length of 15 km to the horizontal slab, shorter than the width of the infinitely long slab in the original 2D model.

The central and side slabs are assumed to have different Cole–Cole parameters, m and τ, representative of a different physical state of the rocks.

From a previous interpretation of Mauriello *et al* (1996, 2004), m and τ play a significant role in the evaluation of IP effects in volcano-geothermal areas. Essentially, m is related to the degree of alteration and mineral particle deposition arising from rock–fluid interactions. To some extent, high values of m are indicative of high volumes of alteration products that occlude the rock's fissures and pores.

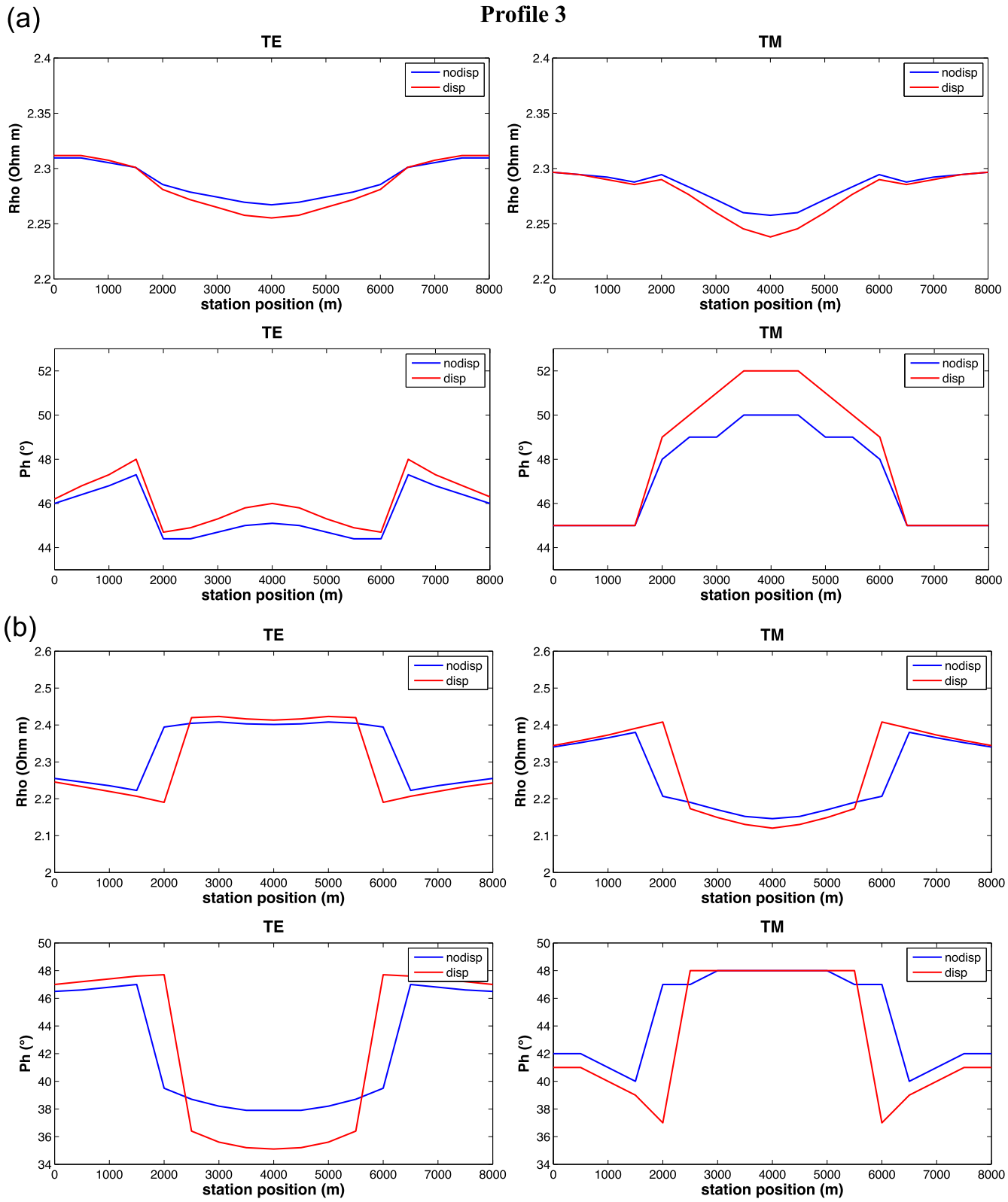

Figure 4. Modulus (top diagrams, in Ω m) and phase (bottom diagrams, in deg) of the two orthogonal TM and TE modes of the MT apparent impedivity response against distance (in m) along profile 3 calculated at various frequencies. The blue curves refer to the reference non-dispersive response, and the red curves to the dispersive case. Frequencies: (a) 10 Hz, (b) 1 Hz, (c) 0.1 Hz, (d) 0.01 Hz, (e) 0.001 Hz.

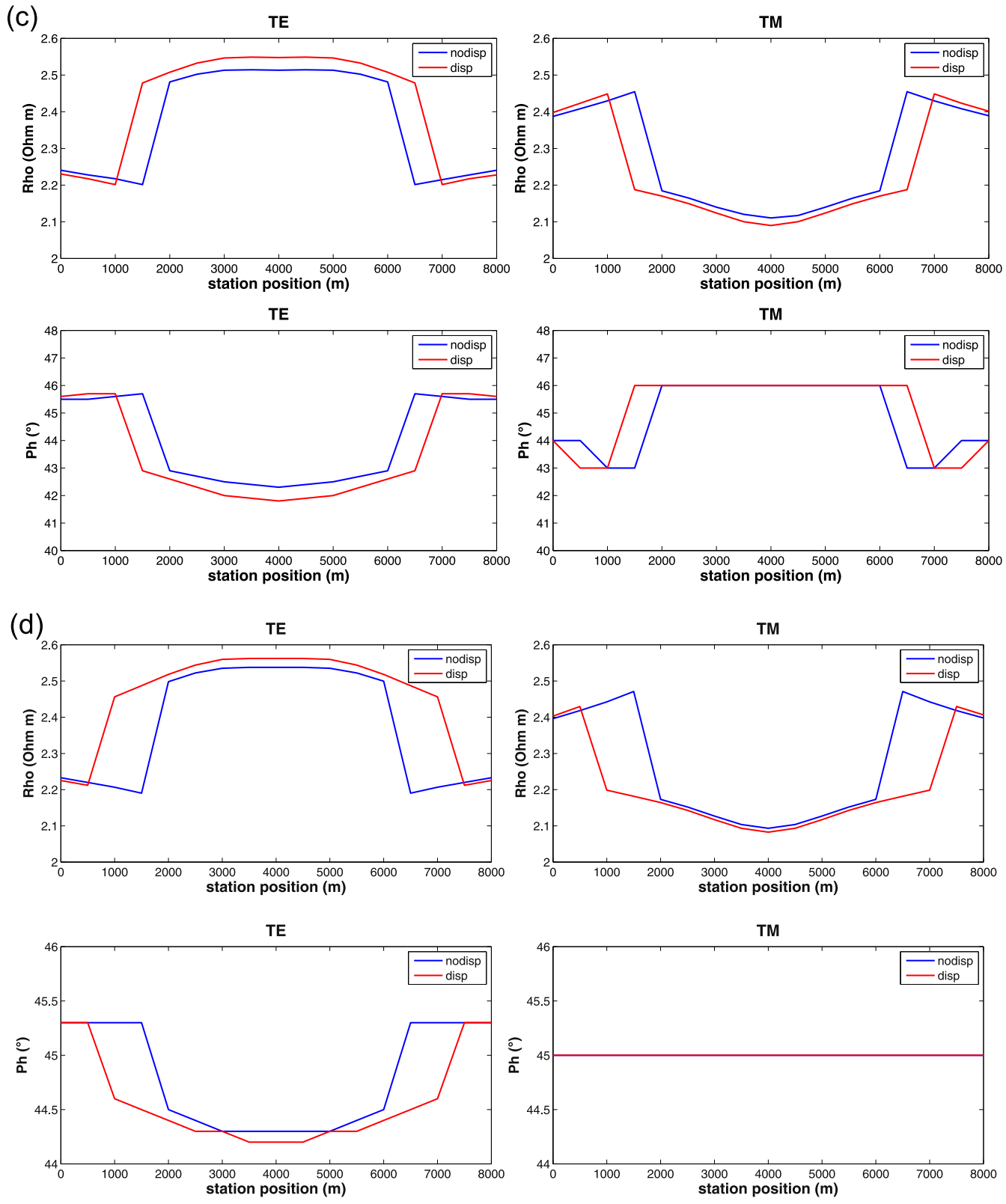

Figure 4. (Continued.)

For the SRP field case examined here, high m values, up to 0.95, have been required to model the MT profile, fully consistent with values found in other volcanic and geothermal environments (Patella *et al* 1991, Di Maio *et al* 2000, Mauriello *et al* 2000, 2004). Instead, from the analysis of other volcano-geothermal systems (Coppola *et al* 1993, Giammetti *et al* 1996, Mauriello *et al* 2004) it appears that the parameter τ is connected to the local temperature, to which it

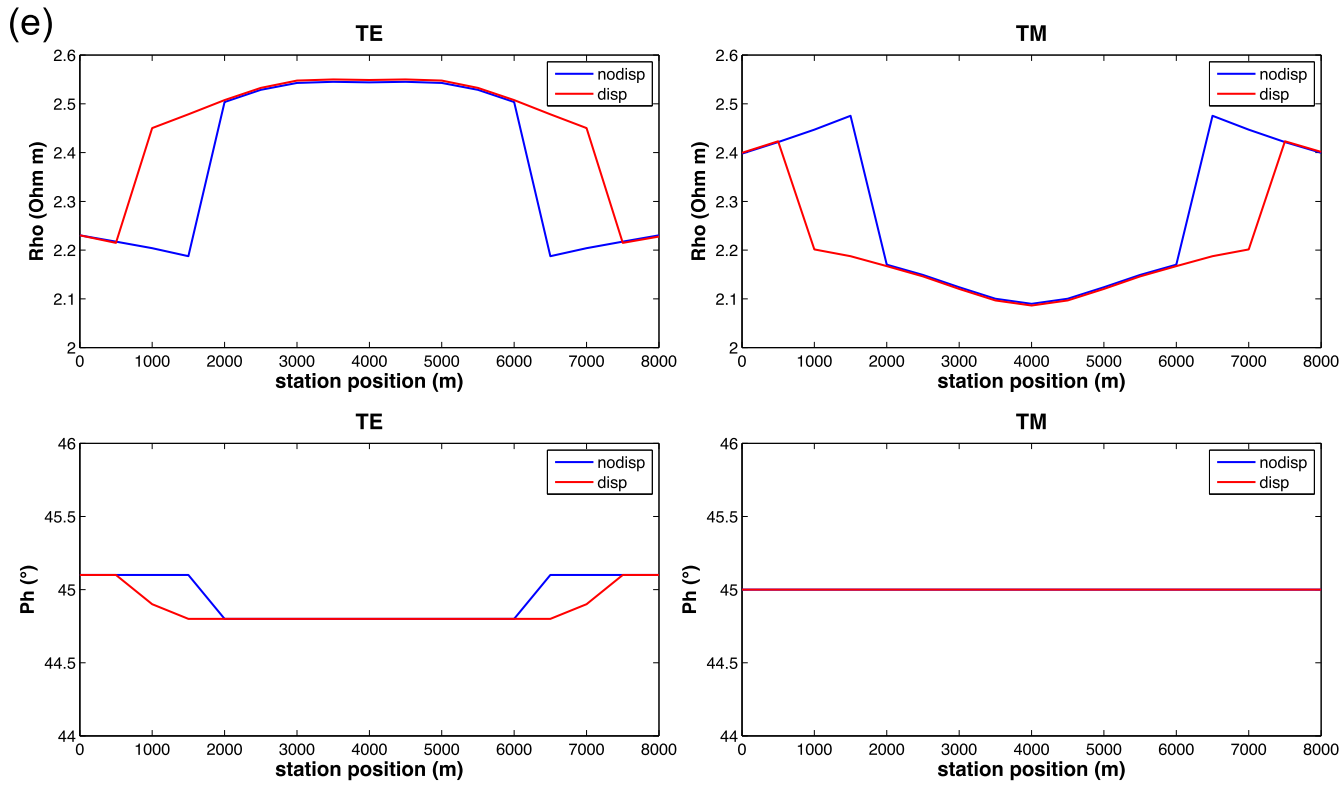

Figure 4. (Continued.)

is correlated through a complex direct proportionality, as shown in the empirical diagram of figure 8.

Therefore, the values of the parameter τ used for the dispersive slabs—$\tau = 15$ s for the side slabs and $\tau = 75$ s for the central one, as reported in figure 7—should indicate temperatures between 70 °C and 125 °C in the central part of the slab and between 50 °C and 90 °C in the side parts, in the depth range 1.5–2.5 km below the SRP depression. These indirect estimates of temperature are in full agreement with data from the INEL-1 test hole, located as in figure 5, where water temperature was found to increase from 26 °C at 600 ft below land surface to 146 °C at 9985 ft, with a nearly linear gradient averaging about 1.3 °C/100 ft of depth (Mann 1986).

Figure 9 shows the TM and TE pseudosections of synthetic apparent resistivity, derived from the new 3D model. Finally, figure 10 shows the misfit between the field and synthetic pseudosections, which has been plotted by assigning at each point of the pseudosections the modulus of the discrepancy index r_i, given by (Troiano *et al* 2014)

$$r_i = |(d_i - m_i)/\varepsilon_i|, \tag{2}$$

where d_i are the observed data, m_i are model responses and ε_i are the data errors with $i = 1, 2, \ldots, N$, and N being the total number of measured data.

The normalized root mean square (rms) misfit has been calculated using the formula (Gabàs and Marcuello 2003)

$$\text{rms} = \sqrt{\left(\sum_N r_i^2 / N\right)}. \tag{3}$$

Average rms values have been obtained equal to 2.6 for the TM section and 3.1 for the TE section.

Conclusion

The present study has analyzed the distortion effects due to resistivity frequency dispersion in the MT response over a 3D structure, consisting of a conductive and dispersive horizontal prism immersed in a resistive, non-dispersive half-space. This type of structure can be very useful for modeling geothermal and hydrocarbon reservoirs, which likely account for the presence of relevant dispersion effects, due to the high degree of alteration produced by the circulation of aggressive fluids. The dispersion effects have been evaluated along three parallel profiles, normal to the longitudinal axis of the prism. Variations in the amplitude and width of the anomaly above the dispersive body have been recognized, depending on the distance of the profile from the center to the edges of the prism.

The field case of the MT profile in the eastern Snake River Plain geothermal area, previously dealt with by a 2D approach, has been reconsidered using a 3D forward modeling that includes dispersion effects. An increased goodness of fit has been obtained between the field TM and TE pseudosections and the synthetic ones derived from the 3D model, compared with the misfit previously obtained by the 2D approach. We thus feel that we can consider the 3D refinement of the original 2D model to be evidence of the greater accuracy that can be reached by a 3D approach to the interpretation of MT data supposed to be affected by dispersive effects.

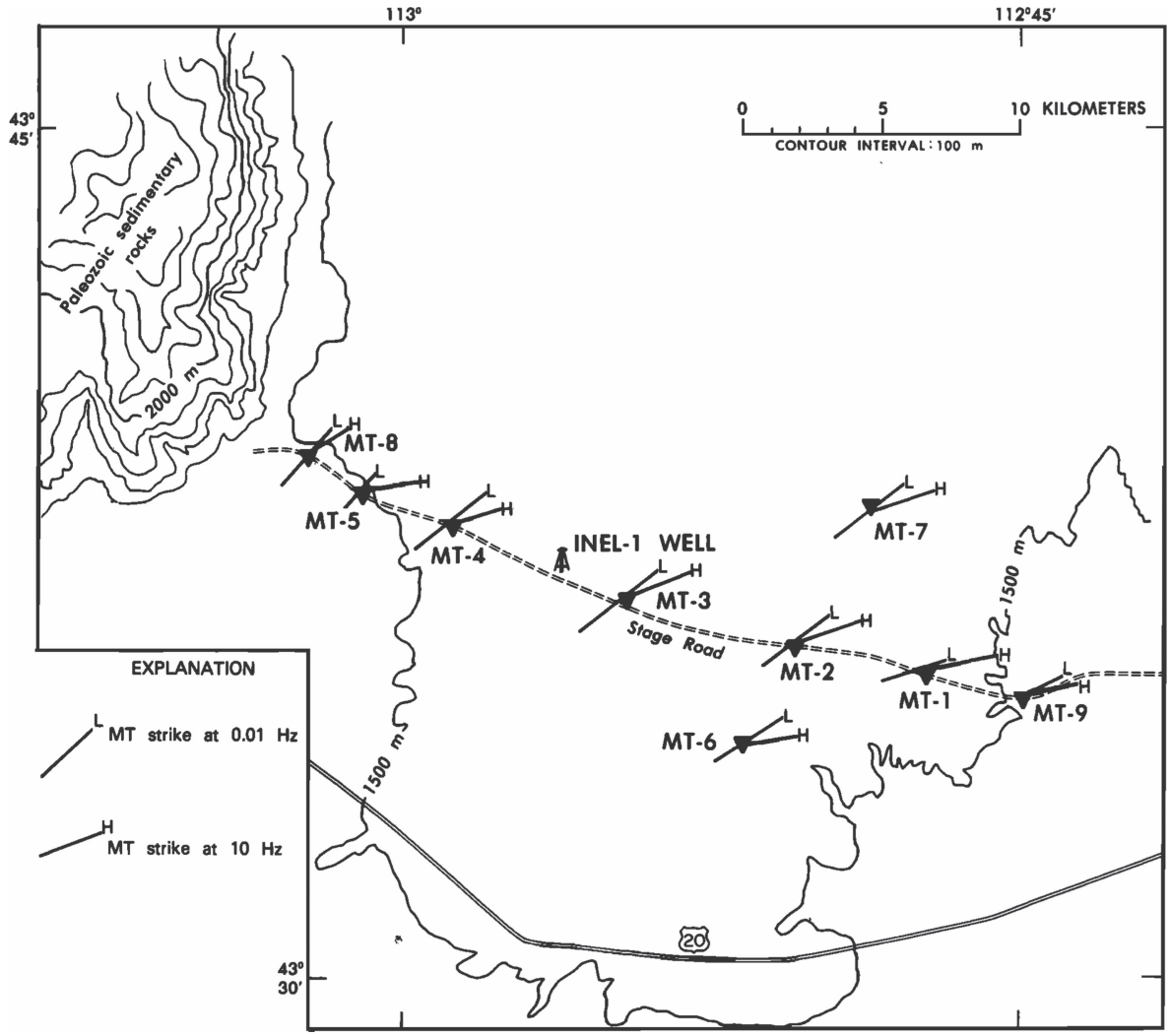

Figure 5. The eastern Snake River Plain with indication of the MT stations along the profile measured by Stanley (1982) and of the INEL-1 test borehole. Redrawn after Stanley (1982), Copyright 1982 by the American Geophysical Union.

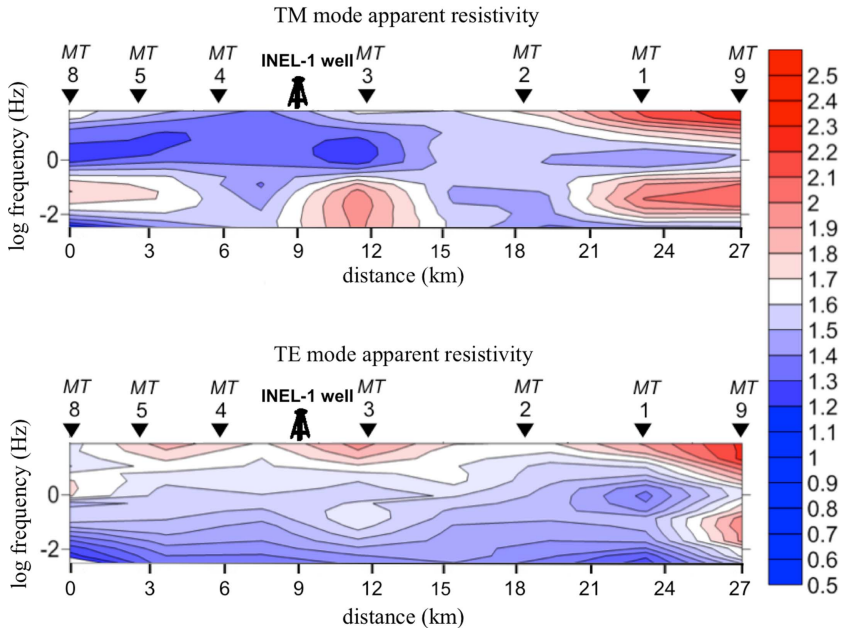

Figure 6. MT TM and TE field pseudosections of the Snake River Plain (redrawn after Stanley 1982). The color scale is in Ω m.

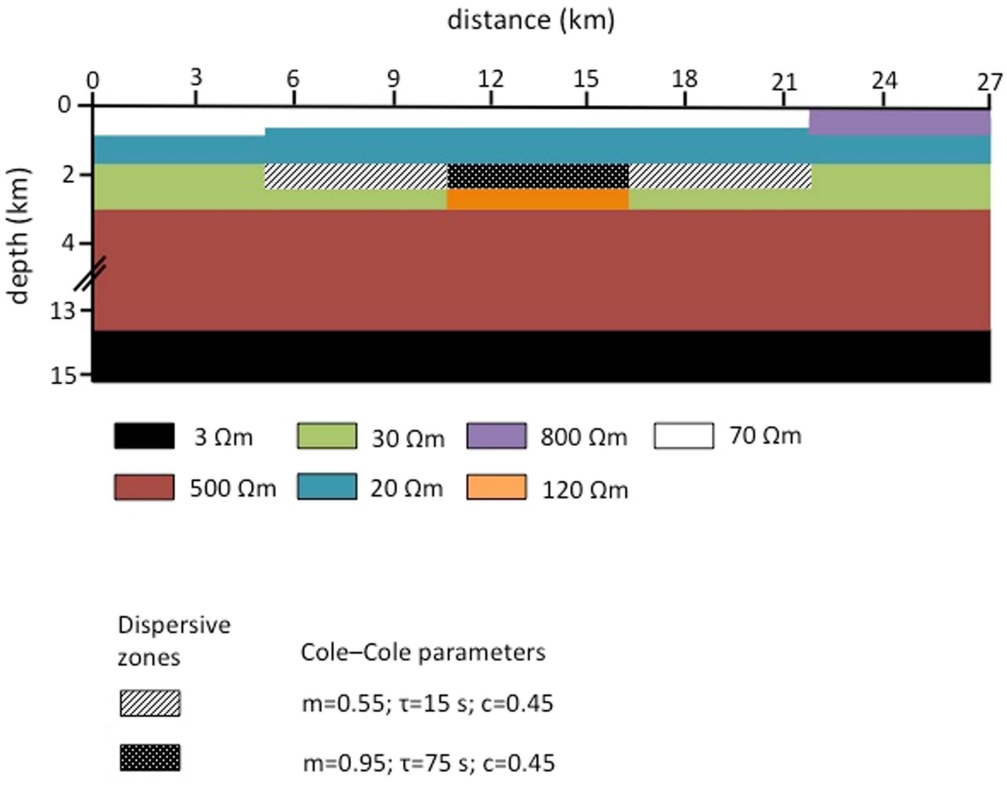

Figure 7. The NW–SE section of the interpreted structural model of the Snake River Plain across the MT profile by Stanley (1982). The 3D conductive slab (15 km wide in the direction normal to the section) is assumed to be affected by resistivity frequency dispersion.

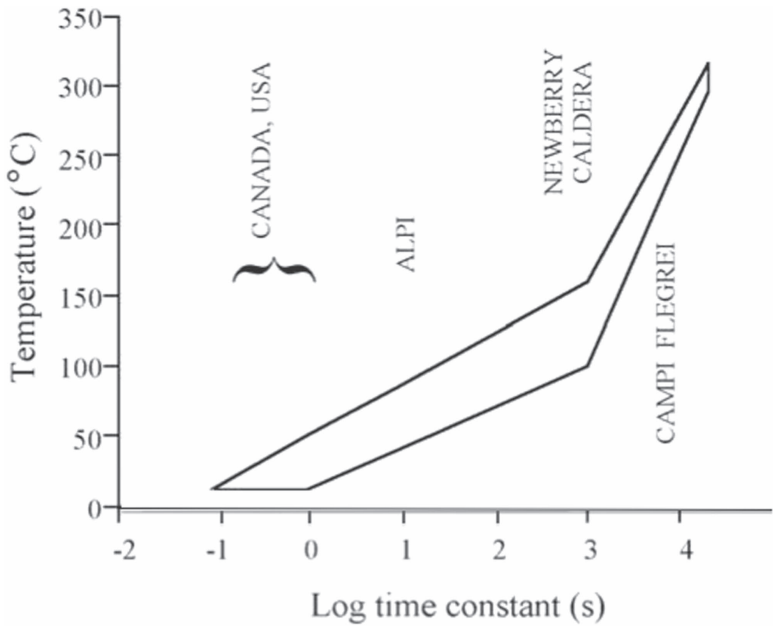

Figure 8. Temperature versus Cole–Cole parameter τ. Reproduced from Mauriello *et al* (2004), Copyright 2004 by the American Geophysical Union.

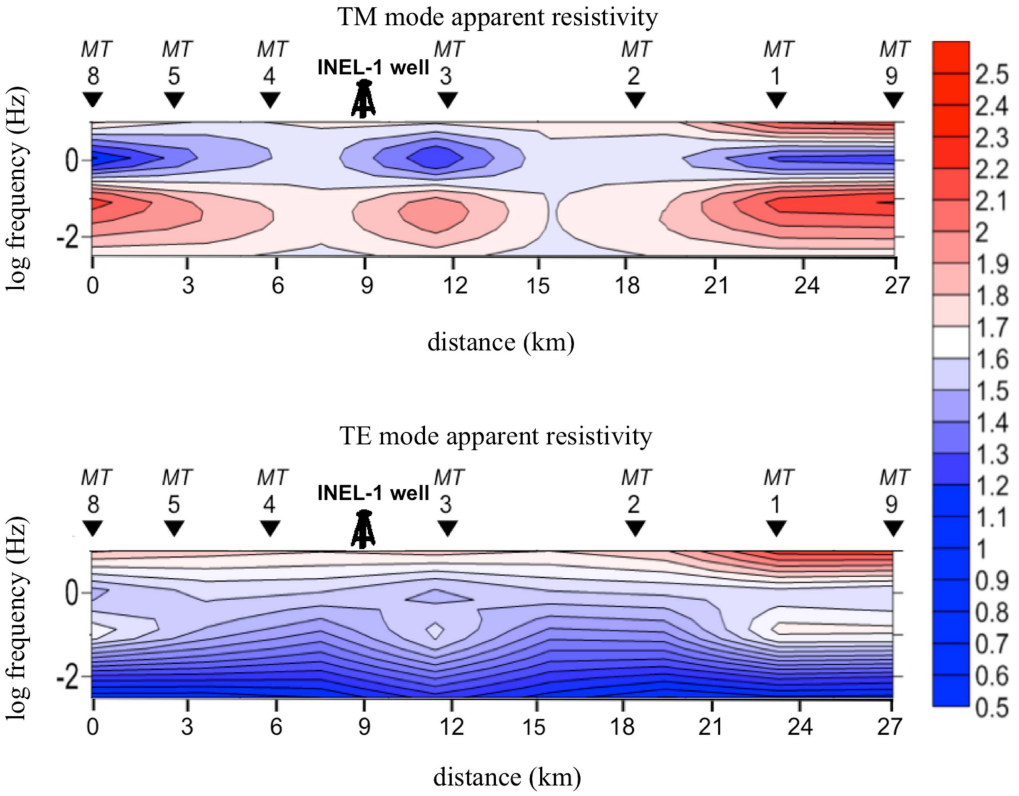

Figure 9. MT TM and TE synthetic pseudosections of the Snake River Plain, reconstructed from the 3D model in figure 7. The color scale is in Ω m.

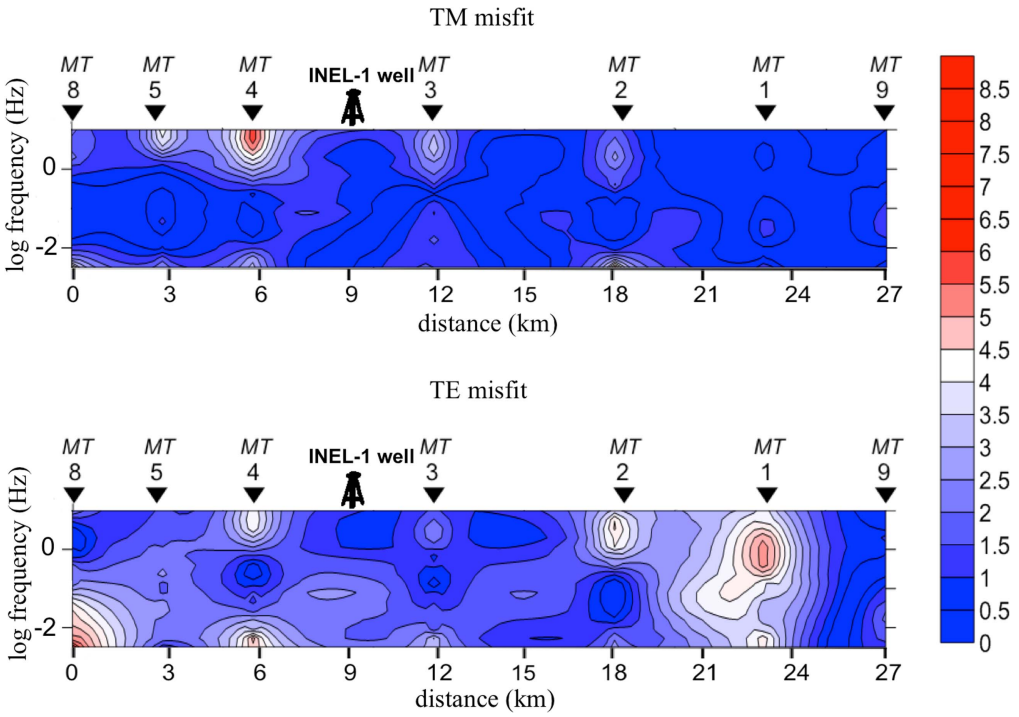

Figure 10. Misfit between the observed MT TM and TE pseudosections drawn in figure 6 and the synthetic ones drawn in figure 9.

References

Bertin J and Loeb J 1976 *Experimental and Theoretical Aspects of Induced Polarization* (Berlin: Gebrüder-Borntraeger)

Chang-Chun Y and Bin L 1994 The research on the 3D TDEM modeling and IP effect *Chin. J. Geophys.* **37** (S2) 486–92

Cole K S and Cole R H 1941 Dispersion and absorption in dielectrics. Part I. Alternating current characteristics *J. Chem. Phys.* **9** 341–51

Coppola B, Di Maio R, Marino I, Merla A, Patella D, Pulelli G, Rossi F M and Siniscalchi A 1993 Study of the Simplon area geothermal anomaly in the frame of a transalpine deep railway tunnel feasibility project *Underground Transportation Infrastructures* ed J L Reith (Rotterdam: Balkema) pp 93–102

Di Maio R, Mauriello P, Patella D, Petrillo Z, Piscitelli S, Siniscalchi A and Veneruso M 1997 Self-potential, geoelectric and magnetotelluric studies in Italian active volcanic areas *Ann. Geophys.* **40** 519–37

Di Maio R, Patella D, Petrillo Z, Siniscalchi A, Cecere G and de Martino P 2000 Application of electric and electromagnetic methods to the study of the Phlegrean Fields caldera *Ann. Geophys.* **43** 375–90

Esposito R and Patella D 2009 The role of the impedivity in the magnetotelluric response *PIER* **89** 225–53

Fink J B, McAlister E O, Sternberg B K, Wieduwilt W G and Ward S H (ed) 1990 *Induced Polarization: Applications and Case Histories, Investigations in Geophysics* vol 4 (Tulsa, OK: SEG)

Gabàs A and Marcuello A 2003 The relative influence of different types of magnetotelluric data on joint inversions *Earth Planet. Space* **55** 243–8

Giammetti S, Patella D, Siniscalchi A and Tramacere A 1996 The Siena Graben: combined interpretation of DES and MT soundings *Ann. Geophys.* **39** 189–200

He Z, Hu Z, Luo W and Wang C 2010 Mapping reservoirs based on resistivity and induced polarization derived from continuous 3D magnetotelluric profiling: case study from Qaidam basin, China *Geophysics* **75** B25–33

Hoheisal A, Hördt A and Hanstein T 2004 The influence of induced polarization on long-offset transient electromagnetic data *Geophys. Prospect.* **52** 417–26

Keller G V and Frischknecht F C 1966 *Electrical Methods in Geophysical Prospecting* (Oxford: Pergamon)

Livelybrooks D, Mareschal M, Blais E and Smith J T 1996 Magnetotelluric delineation of the Trillabelle massive sulfide body in Sudbury, Ontario *Geophysics* **61** 971–86

Mabey D R 1982 Geophysics and tectonics of the Snake River Plain, Idaho *Cenozoic Geology of Idaho* (*Idaho Bureau of Mines and Geology Bulletin* 26) ed B Bonnichsen and R M Breckenridge (Moscow, ID: Idaho Department of Lands, Bureau of Mines and Geology) pp 139–53

Mann L J 1986 Hydraulic properties of rock units and chemical quality of water for INEL-1: a 10,365-foot deep test hole drilled at the Idaho National Engineering Laboratory, Idaho *Water-Resources Investigations Report* 86-4020 (US Geological Survey, Water Resources Division)

Marchant D, Haber E and Oldenburg D W 2014 Three-dimensional modeling of IP effects in time-domain electromagnetic data *Geophysics* **79** E303–14

Mauriello P, Patella D and Siniscalchi A 1996 The magnetotelluric response over two-dimensional media with resistivity frequency dispersion *Geophys. Prosp.* **44** 789–818

Mauriello P and Patella D 1999 Principles of probability tomography for natural-source electromagnetic induction fields *Geophysics* **64** 1403–17

Mauriello P, Patella D, Petrillo Z and Siniscalchi A 2000 An integrated magnetotelluric study of the Mt. Etna volcanic structure *Ann. Geophys.* **43** 325–42

Mauriello P, Patella D, Petrillo Z, Siniscalchi A, Iuliano T and Negro C D 2004 A geophysical study of the Mount Etna volcanic area ed A Bonaccorso *et al Mt. Etna: Volcano Laboratory* (*Geophysical Monograph Series* vol 143) (Washington, DC: AGU) pp 273–91

Patella D 1987 Tutorial: Interpretation of magnetotelluric measurements over an electrically dispersive one-dimensional earth *Geophys. Prosp.* **35** 1–11

Patella D 1993 I principi metodologici della magnetotellurica su mezzi generalmente dispersivi *Ann. Geophys.* **36** (Suppl. 5-6) 147–60

Patella D, Tramacere A, Di Maio R and Siniscalchi A 1991 Experimental evidence of resistivity frequency-dispersion in magnetotellurics in the Newberry (Oregon), Snake River Plain (Idaho) and Campi Flegrei (Italy) volcano-geothermal areas *J. Volcanol. Geoth. Res.* **48** 61–75

Pellerin L, Johnston J M and Hohmann G W 1996 A numerical evaluation of electromagnetic methods in geothermal exploration *Geophysics* **61** 121–37

Pelton W H, Ward S H, Hallof P G, Sill W R and Nelson P H 1978 Mineral discrimination and removal of inductive coupling with multifrequency IP *Geophysics* **43** 588–609

Seigel H O 1959 Mathematical formulation and type curves for induced polarization *Geophysics* **24** 547–65

Stanley W D 1982 Magnetotelluric soundings on the Idaho National Engineering Laboratory facility, Idaho *J. Geophys. Res.* **87** 2683–91

Stoyer C H 1976 Consequences of induced polarization in magnetotelluric interpretation *Pure Appl. Geophys.* **114** 435–49

Sumner J S 1976 *Principles of Induced Polarization for Geophysical Exploration* (Amsterdam: Elsevier)

Troiano A, Di Giuseppe M G, Patella D, Troise C and De Natale G 2014 Electromagnetic outline of the Solafatara-Pisciarelli hydrothermal system, Campi Flegrei (Southern Italy) *J. Volcanol. Geoth. Res.* **277** 9–21

Wait J R 1959 *Overvoltage Research and Geophysical Applications* (Oxford: Pergamon)

Wannamaker P E, Hohmann G W and Ward S H 1984 Magnetotelluric responses of three-dimensional bodies in layered earth *Geophysics* **49** 1517–33

Wannamaker P E, Johnston J M, Stodt J A and Booker J R 1997 Anatomy of the southern Cordilleran hingeline, Utah and Nevada, from deep electrical resistivity profiling *Geophysics* **62** 1069–86

Zaslavsky M, Druskin V and Knizhnerman L 2011 Solution of 3D time-domain electromagnetic problems using optimal subspace projection *Geophysics* **76** F339–51

Zhdanov M S and Keller G V 1994 *The Geoelectrical Methods in Geophysical Exploration* (Amsterdam: Elsevier)